ASTEROIDS AS CALIBRATION STANDARDS IN THE THERMAL INFRARED – APPLICATIONS AND RESULTS FROM ISO

T. G. Müller[1] and J. S. V. Lagerros[2]

[1]ISO Data Centre, European Space Agency, Villafranca del Castillo, P.O. Box 50727, 28080 Madrid, Spain
[2]Astronomiska observatoriet, Box 515, SE-752 37 Uppsala, Sweden

ABSTRACT

Asteroids have been used extensively as calibration sources for ISO. We summarise the asteroid observational parameters in the thermal infrared and explain the important modelling aspects. Ten selected asteroids were extensively used for the absolute photometric calibration of ISOPHOT in the far-IR. Additionally, the point-like and bright asteroids turned out to be of great interest for many technical tests and calibration aspects. They have been used for testing the calibration for SWS and LWS, the validation of relative spectral response functions of different bands, for colour correction and filter leak tests. Currently, there is a strong emphasis on ISO cross-calibration, where the asteroids contribute in many fields. Well known asteroids have also been seen serendipitously in the CAM Parallel Mode and the PHT Serendipity Mode, allowing for validation and improvement of the photometric calibration of these special observing modes.

Key words: Minor planets, asteroids; Standards; Infrared: Solar system

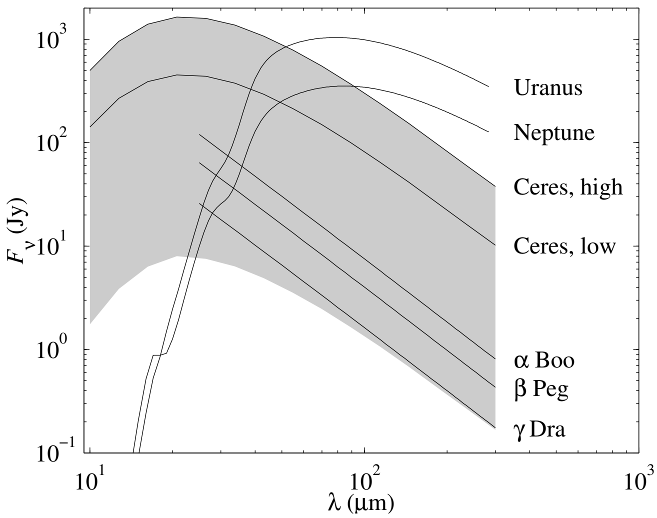

Figure 1. The brightness levels of celestial standards used for the ISOPHOT far-IR calibration (Paper I). The shaded area indicates the approximate flux range covered by the selected asteroids. The changing Earth-asteroid distance causes absolute flux increase or decrease, which is demonstrated by Ceres.

1. INTRODUCTION

With the launch of the Infrared Space Observatory (ISO, Kessler et al. 1996) in November 1995 it has been necessary to establish celestial standards for the calibration of the instruments in the newly opened far-IR range. The emission from stellar photospheres is too faint and the planets are in general too bright in the far-IR. Brighter, dust rich sources, i.e. Ultra-Compact H II regions, protostars, protoplanetary nebulae and AGB-stars surrounded by massive dust envelopes are often embedded in dust clouds which provide a strong and variable background (Sandell 1998). Additionally, modelling proves to be difficult and extrapolations to far-IR wavelengths between 50 and 250 μm are almost impossible.

Asteroid models were already used for IRAS to "transport" the calibration from 60 to 100 μm (Beichman et al. 1988). Also for ISO, they were considered as ideal far-IR standards to fill the flux gap (two orders of magnitude in flux, see Figure 1) and to serve as complements to the hot blue standard stars. Asteroids are point-like and emit the largest fraction of their energy at thermal IR wavelengths. Müller & Lagerros (1998, in the following Paper I) provided a set of 10 asteroids, based on recent thermophysical model code by Lagerros (1996; 1997; 1998). The model input parameters were derived from ground-based mid-IR and submillimetre observations, IRAS and some early ISO data. The quality of the model predictions against ISO data, and their general use as calibration standards, are discussed by Müller & Lagerros (2001, in the following Paper II). These asteroids have then been extensively observed by ISO for photometric calibration, for testing relative spectral response functions and for many technical and calibration purposes.

In the following we summarize the crucial modelling and observational parameters (Section 2). In Sections 3, 4 and 5 we give a detailed overview of all asteroid related calibration applications for ISO and discuss the outcome. With the ISO data it was for the first time possible to test model predictions at far-IR wavelengths. We summarize these results and give conclusions (Section 6) for future projects and for the use of asteroids as calibration sources in the thermal IR.

2. MODELLING AND OBSERVATIONAL ASPECTS

To a zeroth order, the IR brightness is determined by the apparent size and the temperature across the surface. Over the orbital period (3–6 y in the main belt) the changing distance to the Sun will induce temperature variations covering the dynamic range approximately given by $\sqrt{(1+e)/(1-e)}$, where e is the eccentricity of the orbit. From this, the temperatures are typically (17 ± 13) % higher at perihelion than at aphelion.

In principle, the varying distance between the Earth and a main belt asteroid (MBA) typically yields a factor of 5 between minimum and maximum flux density. In practice however, there are constraints on the observing geometry, such as the solar elongation, which significantly reduces the dynamic range resulting from distance scaling. For ISO a factor of 2 was possible for MBAs in some extreme cases, but typical values were significantly smaller.

Asteroids show rotational light-curves, mainly due to the elongated shape and in some cases albedo variations across the surface. For the asteroids larger than 200 km in diameter, the range of periods is 4.2–29 h with a mean of 8.7 h, and the mean amplitude of the visual light curve 0.22 ± 0.15 magnitudes (Lagerkvist, private communication). The amplitude in the thermal IR is comparable to that in the visual, since both are approximately proportional to the projected surface area.

2.1. Thermophysical Modelling

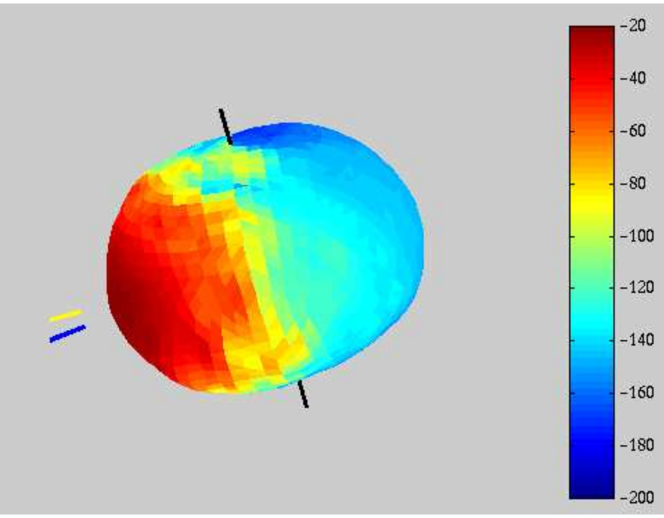

Figure 2. The TPM for Vesta (seen from the side). Temperatures are in [°C].

The precise description of the TPM code used for the 10 ISO asteroids can be found in Lagerros (1996; 1997; 1998). Additionally to the accurate handling of the observing geometry, size and albedo, shape and rotational behaviour of the object, the TPM also treats thermophysical aspects like thermal inertia, beaming and surface roughness and emissivity. The input values for the individual objects were derived in Paper I and are summarised again in Paper II. A demonstration of one possible TPM output (in terms of surface temperature) is given in Figure 2.

2.2. IR Background

The IR background in the ecliptic plane is dominated by zodiacal light and therefore relatively smooth. It can be approximated as diluted black body radiation with temperatures ranging from 259 K ($\lambda - \lambda_\odot = 120°$) to 280 K ($\lambda - \lambda_\odot = 60°$) (Abraham et al. 1999). The background strongly increases at around $\lambda_{ecl.} = 90°$ and $\lambda_{ecl.} = 270°$, where the ecliptic crosses the galactic plane.

At 25 μm the background along the ecliptic plane varies between 60 and 100 MJy/sr (COBE/DIRBE annual maps for $\lambda - \lambda_\odot = 90°$, Hauser et al. 1998) at 140 μm the background values are about 10 MJy/sr, but reaching up to 60 MJy/sr at $\lambda = 90°$ and more than 1500 MJy/sr at $\lambda = 270°$ (close to the galactic centre).

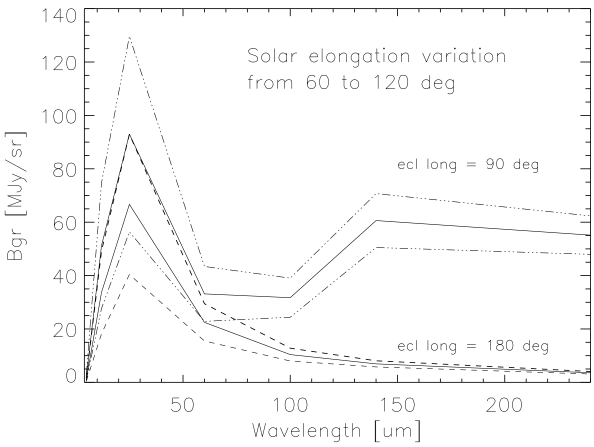

Figure 3. The background spectrum in the ecliptic plane for $\lambda_{ecl.} = 180°$ and $\lambda_{ecl.} = 90°$. The variations for solar elongations between $\lambda - \lambda_\odot = 60°$ and $\lambda - \lambda_\odot = 120°$ are also shown. Values are from COBE/DIRBE weekly maps at the corresponding observing times.

The background of a given position in the ecliptic plane changes with time, depending on the angular distance from the sun (see Figure 3). Under the ISO visibility constraints, between $\lambda - \lambda_\odot = 60°$ and $\lambda - \lambda_\odot = 120°$, the background varied up to a factor of 3. Preferable, low background configurations are therefore between $\lambda_{ecl.} = 0...70°$, 100...250° and at $\lambda_{ecl.} = 280...360°$ for $\lambda - \lambda_\odot > 90°$. Background values of 10, 100 and 1000 MJy/sr correspond to approximately 2, 20 and 200 Jy in a 100″ circular aperture and to 0.02, 0.2 and 2 Jy in a 10″ aperture.

2.3. Apparent Speed and Relative Velocities

Typical MBAs have between 0 and about 80″/hour apparent speed, as seen from the Earth (vector addition of Earth and MBA movement). The ISO motion added in the worst case about 20″/hour at certain points of the 24 h orbit (see Figure 4). In the scientifically useful part of the orbit the speed vector of ISO was typically below 10″/hour.

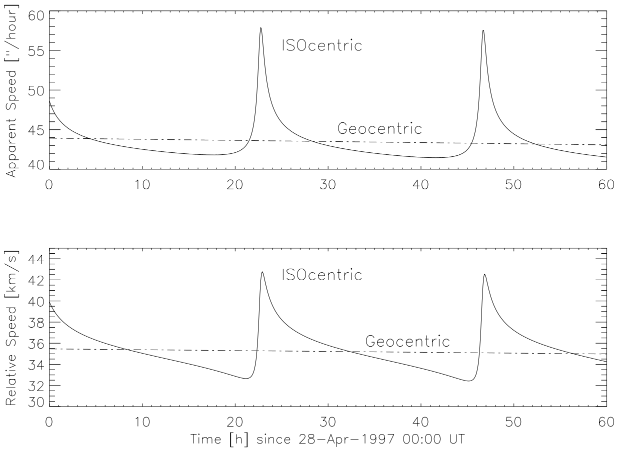

Figure 4. The apparent sky movement [$''$/hour] of the asteroid Vesta with respect to the geocentre and ISO.

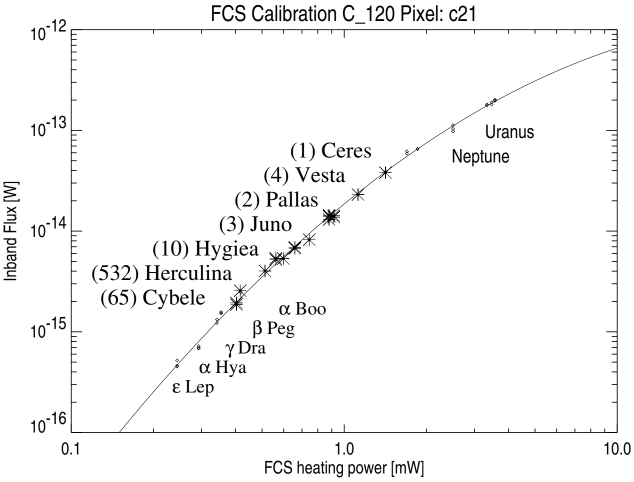

Figure 5. The ISOPHOT calibration of the internal calibration source (FCS) against celestial standards. The stars cover the lowest flux range, the asteroids the intermediate and the planets the high flux range.

Observations of SSOs require accurate, and in some cases, fast, tracking. In the case of ISO, tracking was done as a spacecraft raster with 2$''$ step size, limited to apparent velocities of less than 120$''$/h with respect to equatorial coordinates. This excluded fast moving objects, like a few near-Earth asteroids and comet Hyakutake, from the ISO programme. The relative velocity between typical MBAs and Earth varies between 10 and 50 km/s. The ISO orbit adds an amplitude of about 10 km/s with a 24 h periodicity.

3. PHOTOMETRIC CALIBRATION IN THE FIR

3.1. ISOPHOT

The asteroids 1 Ceres, 2 Pallas, 3 Juno, 4 Vesta, 10 Hygiea, 54 Alexandra, 65 Cybele, 106 Dione, 313 Chaldaea and 532 Herculina were used, together with bright standard stars and the planets Uranus and Neptune, to establish the photometric calibration of ISOPHOT at wavelengths beyond 45 μm (Schulz et al. 1999). Pallas was used also at shorter wavelength, down to 12 μm.

Typically 6 to 8 different asteroids were observed, together with the corresponding backgrounds, in all filters of the P3, C100 and C200 detectors. Most of the measurements were performed in the P99 observing mode in a fixed-time staring configuration together with measurements of ISOPHOT's internal reference source (FCS). Figure 5 shows an example of the photometric calibration of the FCS against celestial standards for one pixel of the C200 camera in the 120 μm filter. The signals of the FCS (expressed in terms of heating power) were ratioed to the signals produced by celestial standards, where the fluxes (or inband powers) were predicted by models.

The photometric calibration of ISOPHOT was established by dedicated measurements of the sources, the backgrounds and the FCS. In this way an absolute photometric calibration accuracy of 10 % (P3), 15 % (C100) and 10 % (C200) was achieved for point sources close to the brightness level of the 10 asteroids (Klaas et al. 2000). Taking the general difficulties of opening a so-far-unexplored wavelength region beyond 100 μm into account, and considering the asteroid shape and thermal modelling aspects, the concept of using asteroids for the absolute calibration worked extremely well. Although the always-changing background conditions for the asteroids required special attention and many dedicated measurements.

3.2. LWS Fixed Grating (L02)

The LWS absolute flux calibration has been established using observations of Uranus in combination with a model of 5 % absolute accuracy (Griffin & Orton 1993). The asteroids were considered as a viable possibility to ensure the calibration, since the brightest stellar standards are already too faint to obtain sufficient S/N values. The bright asteroids provide approximately one tenth of the Uranus flux level (beyond 100 μm), whereas α Boo and α Tau are only at one hundredth of the Uranus brightness. The photometry of LWS has been tested against Ceres, Pallas, Vesta and Hygiea, repeatedly.

The agreement between the calibrated observations and the model predictions, expressed in "Obs/Mod" ratios, is shown in Figure 6. The ratios are close to 1.0 for all detectors and for all objects. Only the detectors SW1 and SW2 show larger deviations (probably due to memory effects) and LW5 has a larger scatter due to dark current uncertainties.

The better flux coverage in the LWS calibration revealed non-linearities in the responses of detectors LW1, LW2 and LW3 (for LW4 and LW5 dark current problems dominated). Going from the bright planets over the asteroids to the faint stars, the responsivity of the detectors changed systematically. The behaviour of LW2 and LW3 compared extremely well with the behaviour of the ISOPHOT stressed Ge:Ga detectors. Empirical correction factors (up to 30 % at lower flux levels and 5 to 15 % for the asteroids) have been derived and have been applied to the observations in Figure 6. Background contribu-

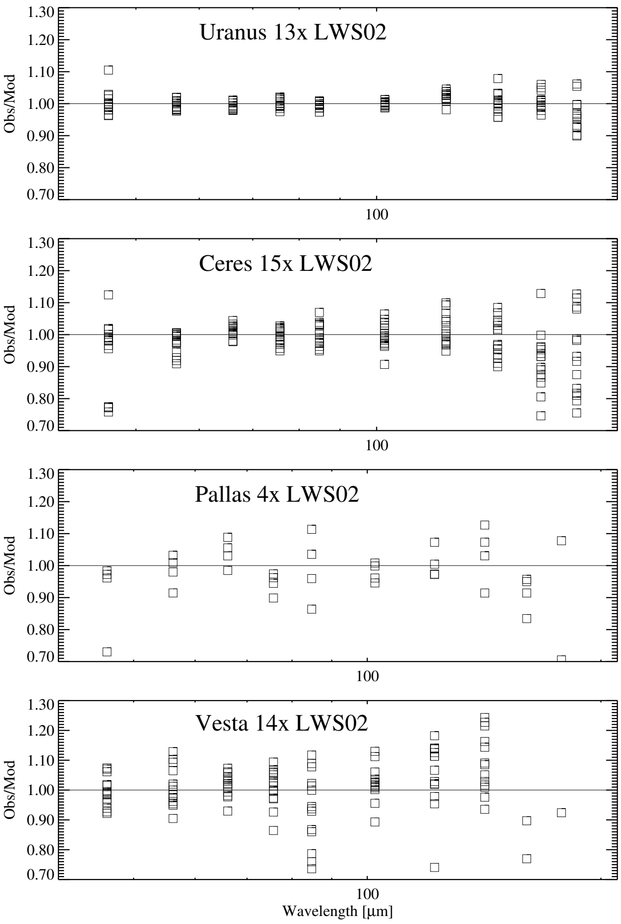

Figure 6. L02 OLP 10 fixed grating measurements of Uranus and 3 asteroids. Observations are divided by the corresponding model prediction. For the asteroids the background contribution had to be subtracted and LW1, LW2 and LW3 were empirically corrected for detector non-linearities.

tions were not important for the bright planets, but had to be considered for the asteroids.

3.3. SWS Flux Calibration

Most of the SWS flux calibration programmes were done on stars which perfectly cover the dynamic range of the detectors, except the highest brightness level beyond 12 μm. Here, bright asteroids and planets were used to check the final photometric calibration (Morris 1999).

The grating flux calibration programme included Ceres, Pallas, Juno, Vesta, Hygiea together with the planets Saturn, Uranus and Neptune. Results are shown in Section 4.

4. RSRF VALIDATION

4.1. SWS (2-45 μm)

The in-flight determination of the relative spectral response function (RSRF) was done on stars. Additionally, the asteroids Ceres, Pallas, Juno, Vesta, Hygiea and the planets Saturn, Uranus and Neptune were observed for testing and validation purposes of the in-flight RSRF.

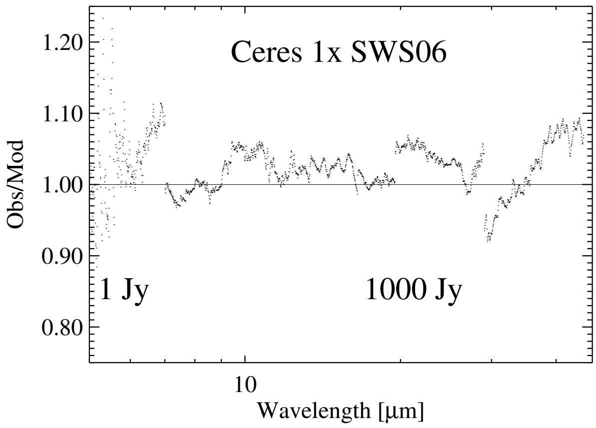

Figure 7. SWS grating scan on Ceres, OLP 10 products, calibrated and tracking-corrected.

Further qualitative comparisons related to spectral features and broad band shapes of the grating RSRF included measurements on Ceres, Pallas, Juno and Hygiea. The errors on the flux calibration of the grating, achieved in orbit, vary between 5 and 30 % at the key wavelengths of the individual bands, increasing with wavelength (Leech et al. 2001). Figure 7 shows the tracking corrected SWS observation of Ceres (1 up- and 1 down-scan per band). Jumps between the individual bands and wrong slopes are still visible at the lower wavelength range.

For the SWS Fabry-Pérot interferometer calibration only measurements on Ceres and Pallas were used in addition to the stars.

4.2. LWS (43-200 μm)

The LWS RSRF has been established on the basis of a Uranus model (Griffin & Orton 1993). Since no prominent lines are known for the asteroids in the LWS wavelength range, they provide independent means to ensure the RSRF calibration. Measurements on Ceres, Pallas, Vesta and Hygiea have been obtained and have partly been used for validation of LWS pipeline products (OLP 10). The Ceres L01 analysis revealed discrepancies in the LWS RSRF of OLP 10 products, which turned out to be caused by an old Uranus model. The L01 results on asteroids confirmed also the detector non-linearities (see Section 3.2).

Figure 8 shows the results of the spectroscopic validation of the grating scans (L01) against Uranus and Ceres. The detector bands SW1, LW1, LW2 and LW3 have been empirically corrected for detector non-linearities, derived from L02 observations of different sources over a large flux range.

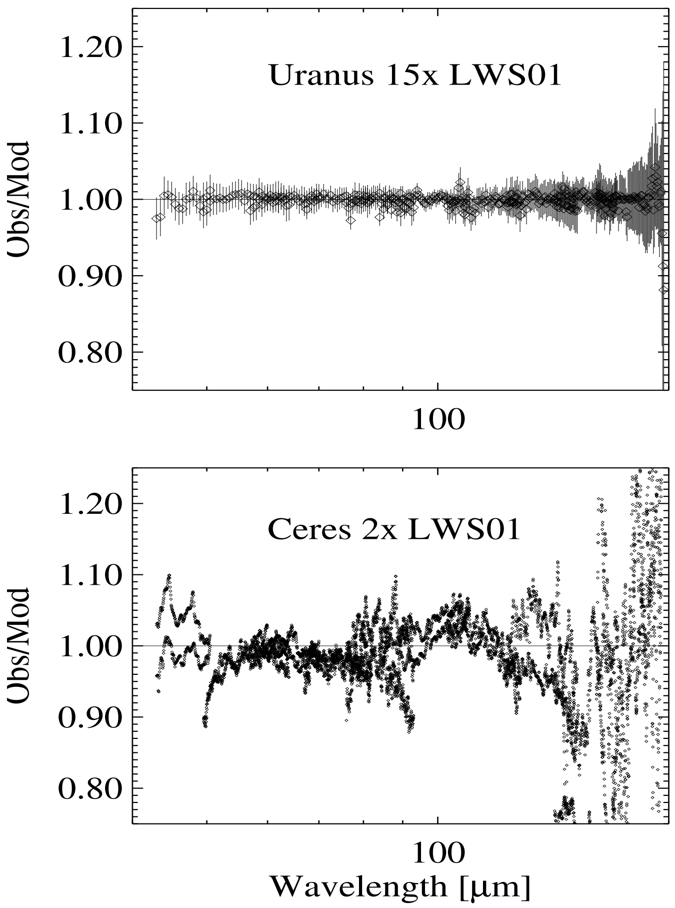

Figure 8. L01 OLP 10 grating scan calibration. Validation against Uranus and Ceres. The error bars for Uranus represent the standard deviation of all 15 scans.

4.3. PHT–S (2-12 μm)

The calibration of PHT–S is based on 24 well known stellar standards, including a few late type K and M giants. Several different asteroids (from calibration and scientific programmes) were used additionally to check the PHT–S data reduction. The calibration of the completely different spectral slope required the combination of many stars at the same time and revealed shortcomings of the early stages of the calibration procedures. It triggered the “dynamic calibration”, where the spectral response function is adapted to the total brightness and transient behaviour of each pixel.

Asteroid spectra with fluxes of 10 to 50 Jy between 7.5 and 9.5 μm, comparable to some late type stars, showed “strange” features in the spectra (Müller et al. 2000). It turned out that the CO and SiO bands of these stars were poorly modelled and the residuals appeared as emission structures in the asteroids.

4.4. CAM–CVF (2-17 μm)

The asteroids Hygiea and Cybele were observed in different CAM modes to compare filter photometry against CVF results for colour correction and filter leak tests (see the contribution by J. Blommaert, in these proceedings).

5. MISCELLANEOUS TOPICS

5.1. TRACKING, BEAM AND APERTURE PROFILES

The apparent sky movements of the asteroids 20 Massalia, 46 Hestia and 56 Melete were used to validate the pointing-tracking system of ISO. Their apparent speed at the time of the measurements were 52.6$''$/hour (Massalia), 28.9$''$/hour (Hestia) and 65.1$''$/hour (Melete). The maximum tracking speed of ISO was 120$''$/hour.

The apparent sky movement of Vesta served in a special calibration programme to characterise the SWS beam profile in the dispersion direction on sub-arcsecond level (with the spacecraft y-axis perpendicular to the asteroid movement). This complemented the extremely time consuming beam profile measurements, which are otherwise done in a series of satellite re-pointings on bright stars. In this way, the satellite pointing uncertainties were reduced from the absolute pointing error (APE) of $< 2.0''$ for each repointing on stars to the absolute pointing drift (APD) of only $< 0.1''$/hour. This method also resolved details of the beam profile at sub-arcsecond level, while the traditional stellar measurements were limited to 2$''$ step size. At the time of the measurement Vesta moved with an apparent speed of approximately 24$''$/hour on the sky.

5.2. COLOUR CORRECTION AND FILTER LEAKS

The accuracy of the photometric calibration depends on the quality of the blocking elements and the characterisation of the band passes. Ceres (in December 1997) and HR 6705 had both approximately 150 Jy flux density at 10 μm. In the case of the asteroid, 10 μm is still on the Wien-part of the spectrum with its intensity peak at around 25 μm. For HR 6705, 10 μm lies on the Rayleigh-Jeans part of the spectrum with its intensity peak in the visible. The measured in-band fluxes are therefore quite different and depend strongly on the width and shape of the band pass. These differences are clearly visible in the colour correction factors, which are calculated for a wide range of sources in comparison to a reference spectrum (ISO used a constant energy spectrum $\nu F_\nu = const.$ as reference).

Table 1. Colour correction factors for blue ($T_{BB} = 5000\,K$) and red sources ($T_{BB} = 200\,K$) for 5 selected ISOPHOT filters.

	Detector-Filter				
T_{BB}	P1_3.6	P1_12	P2_25	P3_60	C100_120
5000 K	1.05	1.30	1.28	1.13	1.21
200 K	1.69	0.89	1.05	1.07	1.17

Table 1 gives an example of colour correction values between typical stellar and asteroid temperatures for different ISOPHOT filters. Indications for filter leaks are given when colour corrected monochromatic fluxes of one source type agree nicely with model predictions, but for the "opposite" source type they do not.

5.3. Special Observing Modes

ISOPHOT Serendipity Mode: During satellite slews the long-wavelength channel of the photometer was used to scan the sky. This ISOPHOT Serendipity Mode (e.g. Stickel et al. 1999) led to a partial sky survey, covering approximately 15 % of the sky, at wavelengths of 170 μm. The first photometric calibration of the Serendipity Mode was based on the results from a small mini-survey. A small area in the sky was mapped in a conventional way and point-source photometry was obtained (Stickel et al. 1998). Later on, a large number of arbitrary slews was done artificially in the same region. The photometric results from the slew data were then compared to results from the conventional photometry, leading to flux correction factors depending on the source brightness and impact parameters.

The bright asteroids, seen serendipitously during the ISO slews, allowed now for a flux calibration in a direct way, using TPM predictions (Müller et al, in preparation). This procedure improved the calibration significantly and extended the calibrated flux range to higher brightness levels, where many new galactic and extragalactic sources have been found (Stickel et al. 2000).

CAM Parallel Mode: Only one ISO instrument was operational in prime mode at a time. However, when the camera was not the main instrument, it was used in parallel mode to acquire extra astronomical data (Siebenmorgen et al. 2000). First analysis of the survey on a small subsample included, by chance, the asteroid 729 Watsonia. Simple model calculations based on IRAS diameter and albedo (Tedesco et al. 1989) gave a flux density of 100$\pm$10 mJy at 6.75 μm. This was in good agreement with the ISOCAM photometry (F_ν =115$\pm$15 mJy). Further photometric analysis on other asteroids are under way, although the final calibration will be based on stars.

LWS Parallel and Serendipity Mode: LWS performed parallel (Lim et al. 2000) and serendipitous surveys (Vivarès et al. 2000) in the far-IR at 10 wavelengths between 46 and 178 μm. As in the case of the ISOPHOT Serendipity Mode, the serendipitously seen planets and bright asteroids can serve as direct calibration standards. The two LWS surveys just underwent a first data processing and could therefore not be analysed at time of writing.

5.4. Cross-Calibration

The bright and point-like asteroids have been used in many cross-calibration aspects. They were intermediate in terms of flux (between stars and planets), intermediate in terms of wavelength (allow the connection from mid-IR to the submillimetre) and bright enough to be observed by all four ISO instruments. Many connections to IRAS (Paper I), to the KAO (Müller et al. 2000) and between ISO sub-instruments (e.g. Paper II or Barucci et al. 2002) have been established via individual asteroids. Examples for interrelation of instrument submodes via asteroids are: S01/S06, P32/P25/P22, P03/P40, L01/L02. The asteroid data can also be used to connect stellar model extrapolations at far-IR wavelength to the planetary models. Work in this area is ongoing. Cross-calibration on asteroids observed at different epochs are always connected to model predictions, and can be combined in "Obs/Mod" ratio plots. More results are presented in the "ISO Post-Operations Cross-Calibration Status Reports", available from the ISO homepage (http://www.iso.vilspa.esa.es) and in the contribution from García (these proceedings).

6. Conclusions

Stellar Standards are excellent calibration standards at near-IR and mid-IR wavelengths. Nevertheless, asteroids provide means to check the photometric calibration and colour correction procedures and to find filter leaks (see also Paper II). Additionally, the RSRF can be validated at critical areas, e.g. in the case of late type stellar standards at the CO and SiO fundamental absorption bands.

In the far-IR the well known MBAs are difficult to beat: being point-like, bright, predictable with high accuracy and no spectral features makes them ideal references for photometric, spectroscopic and technical calibration aspects. The planets, mainly Uranus and Neptune, are, for most of the applications in the far-IR, already too bright. The typical stellar calibrators, on the other hand, provide only low fluxes, and together with the high and structured far-IR background, the source-to-background contrast was therefore not sufficient for most of the technical tests.

Limitations for asteroid measurements are due to the changing background conditions and the flux changes on timescales of hours (due to rotation), which have to be considered in setting up calibration programmes. The apparent sky movements of asteroids are perfectly predictable and can even be used in the beam/aperture profile context in an advantageous way.

The list of reliable asteroids is still short, but can be extended, depending on the needs of future far-IR and submillimetre projects. The most important selection criteria for additional sources would be: Knowledge of absolute size, albedo, shape, spin vector solution and preferably small amplitudes in the light curve.

Acknowledgements

We thank Cecile Gry, Martin Burgdorf, Bernhard Schulz (ISO Data Centre in Villafranca), Fred Lahuis (Dutch ISO Data Analysis Centre) and Tanya Lim (Rutherford Appleton Laboratory) for helpful discussions and support in LWS, SWS and ISOPHOT data reduction.

REFERENCES

Abraham, P., Leinert, C., Acosta-Pulido, J. A. et al., 1999, ESA SP-427, P. Cox & M.F. Kessler (eds.), 261

Barucci, M. A., Dotto, E., Brucato, J. R. et al., 2002, Icarus, 156, 202

Beichman, C. A., Neugebauer, G., Habing, H. J., Clegg, P. E., Chester, T. J., 1988, Infrared astronomical satellite (IRAS) catalogs and atlases. Vol. 1: Explanatory supplement

Griffin, M. & Orton, G.S., 1993, Icarus 105, 537

Hauser, M.G., Kelsall, T., Leisawitz, D. & Weiland, J. (eds.), COBE Diffuse Infrared Background Experiment (DIRBE) Explanatory Supplement, 1998, Vers. 2.3, COBE Ref. Pub. No. 98-A

Kessler, M.F., Steinz, J.A., Anderegg, M.E. et al., 1996, A&A 315, L27

Klaas, U., Laureijs, R. J., Radovich, M., Schulz, B., Wilke, K., 2000, ISOPHOT Calibration Accuracies, ESA SAI/1998-092/Dc

Lagerros, J. S. V., 1996, A&A 310, 1011

Lagerros, J. S. V., 1997, A&A 325, 1226

Lagerros, J. S. V., 1998, A&A 332, 1123

Leech, K., de Graauw, T., van den Ancker, M. et al., 2001, The ISO Handbook: SWS – The Short Wavelength Spectrometer, ESA SAI/2000-008/Dc, Vers. 1.1

Lim, T., Vivarés, F. & Caux, E., 2000, D. Lemke, M. Stickel & K. Wilke (eds.), In: ISO Surveys of a Dusty Universe, Springer, 291

Morris, P., 1999, SWS Photometric Calibrations at EOM, ESA, ISO internal report

Müller T.G. & Lagerros J.S.V., 1998, A&A 338, 340

Müller, T.G., Dotto, E. & Barucci, A., 2000. In: A. Salama, M.F. Kessler, K. Leech, B. Schulz (eds.), ESA SP-456, 33

Müller, T. G. & Lagerros J.S.V., 2002, A&A, 381, 324

Sandell, G. & Aspin, C., 1998, A&A 333, 1016

Schulz, B., Huth, S., Kinkel, U. et al., 1999. In: P. Cox & KM.F. Kessler (eds.), ESA SP-427, 89

Siebenmorgen, R., Schartel, N. & Ott, S., 2000. In: D. Lemke, M. Stickel & K. Wilke (eds.) ISO Surveys of a Dusty Universe, Springer, 275

Stickel, M., Bogun, S., Lemke, D. et al., 1998, A&A 336, 116

Stickel, M., Lemke, D., Toth, L. V. et al., 1999. In: P. Cox & M.F. Kessler (eds.), in ESA SP-427, 839

Stickel, M., Lemke, D., Klaas, U. et al., 2000, A&A 359, 865

Tedesco, E. F., 1989. In: Binzel, Gehrels, Matthews (eds.) Asteroids II (Arizona Press), 1090

Vivarés, F., Lim, T., Day, T. & Caux, E., 2000. In: D. Lemke, M. Stickel & K. Wilke (eds.) ISO Surveys of a Dusty Universe, Springer, 299